33.5324.00/06/03 Confidential

REPORT

Rock mechanical tests of shale samples from the cap rock of the Utsira Sand in well 15/9-A11

- A contribution to the Saline Aquifer CO_2 Storage (SACS) project

Angelamaria Pillitteri, Pierre Cerasi, Johannes Stavrum, Peter Zweigel and Reidar Bøe

www.sintef.no

SINTEF Petroleum Research
July 2003

SINTEF

SINTEF

SINTEF Petroleumsforskning AS
SINTEF Petroleum Research

NO-7465 Trondheim

Telephone: (+47)73 59 11 00
Fax: (+47)73 59 11 02 (aut.)

Enterprise No.:
NO 936 882 331

REPORT

TITLE

Rock mechanical tests of shale samples from the cap rock of the Utsira Sand in well 15/9-A11 – A contribution to the Saline Aquifer CO_2 Storage (SACS) project

AUTHOR(S)

Angelamaria Pillitteri, Pierre Cerasi, Johannes Stavrum, Peter Zweigel and Reidar Bøe

CLASSIFICATION	CLIENT(S)
Confidential	Statoil, SACS consortium, NFR-KLIMATEK
REPORT NO. 33.5324.00/06/03	

REG. NO.	DATE	PROJECT MANAGER	SIGN.
2003.038	7 July 2003	Peter Zweigel	*Peter Zweigel*
NO. OF PAGES	NO. OF APPENDICES	LINE MANAGER	SIGN.
28	2	Torleif Holt	*Torleif Holt*

SUMMARY

Weakly consolidated shale samples from a core from approximately 785 m bsl from well NO15/9A11 were mechanically tested and petrographically characterised. The tested rocks are from the Pliocene Nordland shale which constitutes the cap rock of the CO_2 depository in the Sleipner field area.

Macroscopic characterisation indicates weak bedding only, clay or silt lithology, and weak consolidation. XRD analysis yielded approximately 25 % quartz and approximately 55 % clay minerals. The samples have a density of approximately 2.1 g/cm^3 and approximately 35% porosity.

Three triaxial and one K_0 tests were carried out, of which one triaxial test failed due to fines migration. The successful triaxial tests revealed an almost elastic-perfectly plastic behaviour and yielded Young's moduli of 0.19 and 0.29 GPa and Poisson's ratios of 0.25 and 0.18. The K_0 test provided estimates of the *in situ* vertical and horizontal effective stresses of 9 MPa and 5 MPa, respectively. The value for the *in situ* vertical effective stress differs from an estimate from an overburden density model, which yielded 6 – 7 MPa. One explanation for the difference may be the load effect of a potential previous ice sheet.

KEYWORDS ENGLISH	KEYWORDS NORWEGIAN
North Sea	Nordsjøen
Sleipner field	Sleipnerfeltet
Carbon dioxide storage	Karbondioksidlagring
Rock mechanics	Bergmekanikk
Shale seal	Forseglingsegenskaper til skifer

Table of Contents

1. Introduction, background

At the Sleipner field in the North Sea, CO_2 is separated from natural gas and stored in the underground at a rate of approximately 1 Million ton CO_2 per year. CO_2 is injected near the base of the highly porous and highly permeable Utsira Sand, through which it rises buoyancy-driven upwards towards its seal, the shales of the Nordland Group. Thin shale-layers in the Utsira Sand provide migration barriers and baffles, but most of the injected CO_2 is expected to ultimately accumulate beneath the top seal of the formation.

Previous work in the Saline Aquifer CO_2 Storage (SACS) project based on XRD analyses of cuttings samples from the Nordland Shales in the Sleipner area (Bøe & Zweigel 2001, Kemp et al. 2001, 2002) suggested that migration of CO_2 through the matrix pore network of the samples is not likely. However, time-lapse seismic data indicates that some CO_2 has penetrated through a 6.5 m thick shale package within the Utsira Sand (Arts et al. 2003). According to wire-line log data, this shale package has a similar lithology as the Nordland Shales.

Any assessment of the likelihood for the presence of microfractures, or for the risk for injection-related fracturing in the seal rock, e.g. as a consequence of increased subsurface pore pressure due to the density difference between formation water and CO2, requires rock mechanical data on the seal formation. Accordingly, rock mechanical tests on Nordland Shale rocks from Sleipner were carried out when a core became available due to combined efforts of the Sleipner license and the SACS project. Similar, and partly complementary, tests are being carried out by BGS.

The Nordland Shale core from well NO15/9-A11 is one of very few cores from the Pliocene shale sequence in the shallow subsurface of the North Sea. The single other core from this interval known to us is from well 2/4-C11 in the Ekofisk area (for petrographic data for that core see Lindgren et al. 2002). Drilling problems in the Nordland Shales are not uncommon, and results from the rock mechanical tests documented here may accordingly serve for drilling-related considerations, too.

2. Samples

The following core sections from well NO15/9-A11 were delivered to SINTEF:

1) 907.80 – 908.80 m MD (corresponding to 783.96 – 784.70 m TVDss)
2) 911.60 – 912.60 m MD (corresponding to 786.77 – 787.50 m TVDss)
3) 912-60 – 913.10 m MD (corresponding to 787.50 – 787.87 m TVDss)

The cores were delivered in humid condition.

According to the deviation survey (data provided by Oddvar Bøe, Statoil, email from 30. 08. 2002), the well has at coring depth a deviation from vertical of approximately 42°, i.e. an inclination of approximately 48°.

The top of the Utsira Sand (i.e. the top of the sand wedge at its top) is in the well area at approximately 810 to 816 m (according to depth maps in Zweigel & Hamborg 2002).

Samples for rock mechanical tests were selected based on the expected stability and coherence of the samples. Macroscopic inspection aided by tomographic pictures provided by Statoil, served for the selection.

3. Macroscopic sample description

The core segments were macroscopically inspected and photographed. The photographs are provided in Chapter 8 (Appendix A)

Section 1 (907.80 – 908.80 m MD)
Clay and/or silt. Grey. Very homogeneous, no indications for bedding visible (Figure 8.1, Figure 8.2). Contains small mica flakes. Some shell fragments present, up to 5 mm in diameter.
A core fragment shows planar fabric parallel to the core axis (Figure 8.3, Figure 8.4). No fabric oblique to axis (e.g. bedding) visible.
Straight core, slightly undulating at lower end (Figure 8.5).

Section 2 (911.60 – 912.60 m MD)
Clay and/or/silt. Dark grey. Slight indications for bedding by aligned blackish spots (at 50˚ to core axis) (Figure 8.6, Figure 8.7). Some coarse rock grains (diameter up to 3 mm) in clay matrix. One fracture parallel to bedding (53˚ to core axis; Figure 8.8). Core contains a hole (approx. 2 cm diameter and 3-4 cm depth close to lower end (Figure 8.8).
Undulating core (damaged during coring).
Sample #1 for biostratigraphy taken from fracture part at 912.35 m MD and sent to Tor Eidvin (Norwegian Petroleum Directorate).

Section 3 (912-60 – 913.10 m MD)
Lithology as Core 2. Photograph see Figure 8.9
Fracture with slip line; fracture plane at angle 52˚ to core axis (Figure 8.10). Slip line is in virtual dip orientation (at largest angle between fracture and core) and is therefore interpreted to be probably a coring artefact.
Sample #2 for biostratigraphy taken from fracture part at 912.78 m MD and sent to Tor Eidvin (Norwegian Petroleum Directorate).

4. XRD and related analyses

Two samples, one from the upper and one from the lower core segment, were analysed by XRD. Sample preparation and analytical procedure are as described in Bøe & Zweigel (2001). Results from whole rock analysis are listed in Table 4.1 and shown in Figure 4.1 and Figure 4.2. Results of fine fraction analysis (<4μm) are presented in Table 4.2.

In the course of the preparation procedure, samples were dried, which allows to determine wet and dry density, water content and porosity (Table 4.3). The porosity values indicate that the samples were well preserved and were not dried out prior to analysis.

Table 4.1 Semi-quantitative mineral composition (weight percentages) of two samples from well 15/9-A11.

Depth (m)	Qtz	K-fsp	Plag	Chl	Kaol	Mic/Ill	ML	Sme	Cc	Sid	Dol/Ank	Pyr	Amph
907.8	24.1	3.3	7.1	3.6	26.4	25.9	2.2	1.1	2.2	3.0	0.0	0.8	0.4
912.6	27.7	3.4	8.3	3.0	18.3	29.7	1.9	1.8	0.5	3.2	0.0	1.5	0.8

Qtz: Quartz, K-fsp: K-feldspar, Plag: Plagioclase, Chl.: Chlorite, Kaol.: Kaolinite, Mic/Ill: Mica and Illite, ML: Miced Layer Clay, Sme: Smectite, Cc: Calcite, Sid: Siderite, Dol/Ank: Dolomite and Ankerite, Pyr: Pyrite, Amph: Amphibole

Table 4.2 Semi-quantitative mineral composition (weight percentages) of the fine fraction (<4μm) two samples from well 15/9-A11. For abbreviations see Table 4.1.

Depth (m)	Qtz	K-fsp	Plag	Chl	Kaol	Illite	ML	Sme	Cc	Sid	Dol/Ank	Pyr
907.80	4.2	1.5	2.0	5.9	42.2	37.6	0.1	4.1	1.0	1.1	0.0	0.3
912.60	7.9	0.8	2.6	8.5	28.9	39.1	0.3	9.2	0.8	0.9	0.0	0.9

Table 4.3 Wet and dry density, water content, and porosity of the shale samples from well 15/9-A11 that were used for XRD analysis.

Depth (m)	Density wet g/cm^3	Density dry g/cm^3	Weight % H2O	Porosity (%)
907.8	2.086	1.73	17.0	35.5
912.6	2.139	1.80	15.7	33.7

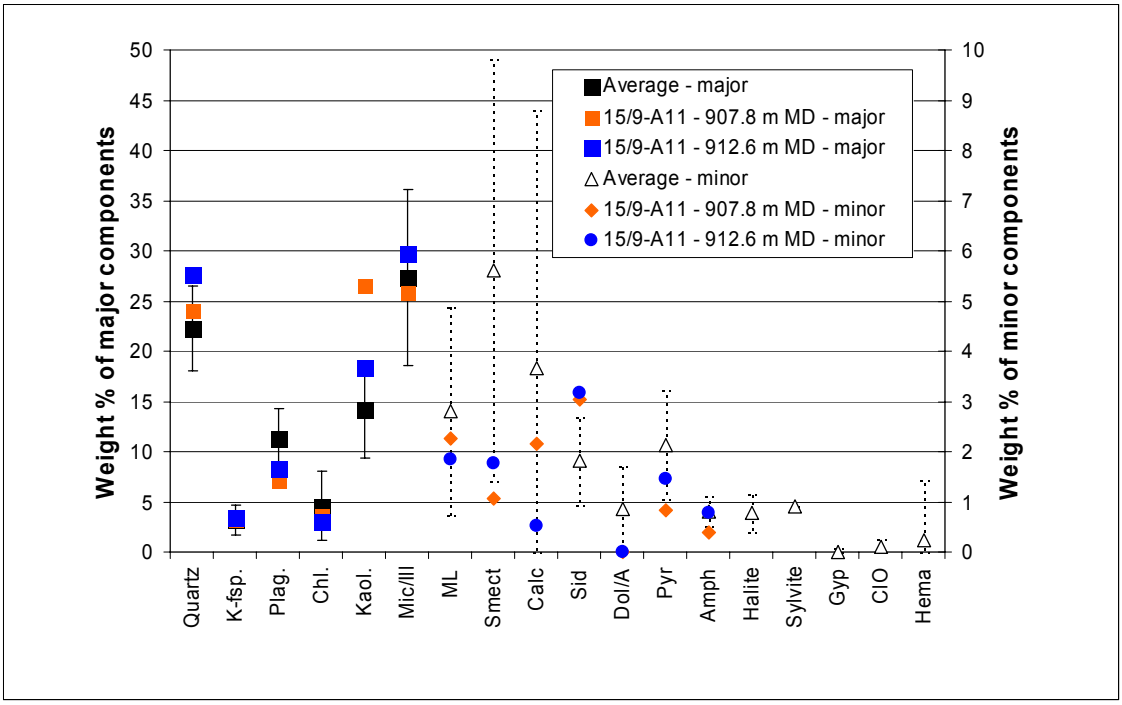

Figure 4.1 *Mineralogical rock composition from XRD analyses of the core segments at SINTEF compared to the average and standard deviation of previous XRD analyses from other segments of the same core (Kemp et al. 2002) and from the Sleipner area (Bøe & Zweigel 2001).*

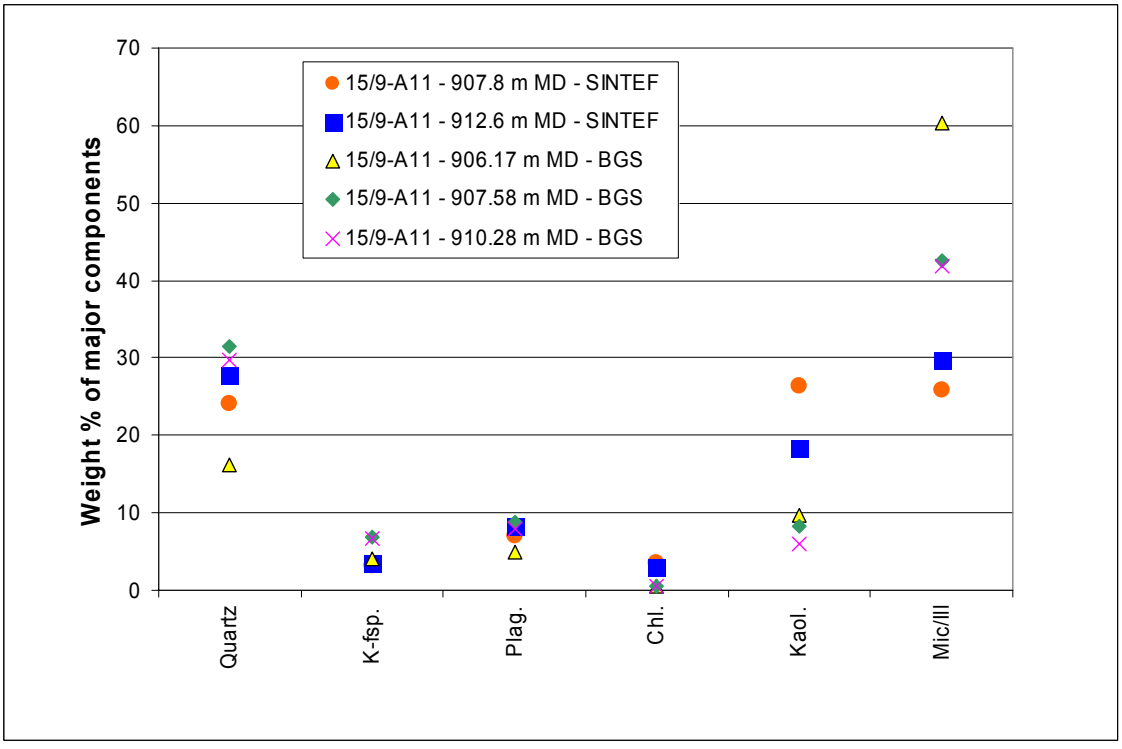

Figure 4.2 *Mineralogical rock composition (main components) from XRD analyses of the core segments at SINTEF compared to results from XRD analyses from other segments of the same core (Kemp et al. 2002).*

5. Rock mechanical tests

5.1 Test procedure

Three triaxial tests and one K_0 test were run in order to characterize the mechanical properties of the material and to estimate the *in situ* horizontal stress.

Tested core dimensions were: diameter 37 mm (11/2 “) and starting length about 70 mm. Cores were cut with axis perpendicular to bedding, in order to reproduce the *in situ* orientation.

Axial deformations during test were controlled by two Linear Variable Differential Transformers (LVDT) and radial deformations by 2(3) radial callipers.

Loading rate during first phase hydrostatic loading was 5-10 MPa/h. Pore pressure was raised until the established value and controlled at the same value.

Consolidation stress was maintained overnight. Pore pressure was kept constant until the beginning of the triaxial phase.

Consolidated, undrained triaxial phase

Loading rate during triaxial phase for the consolidated undrained triaxial tests was estimated case by case from the behaviour during compaction.

Tests were ended according to standard procedure. Effective axial tress is increased until the residual strain is found to be constant or when a perfect plastic behaviour is detected.

K_0 phase

Effective axial stress was increased until 10 MPa and confining pressure was simultaneously steered in order not to allow any lateral deformation. The test was carried out in undrained condition.

Test parameters used for each test are reported in Table 5.1. Tests 1 - 3 are CU triaxial and test 4 is a K_0 test.

Table 5.1 Test parameters for SACS-shales from well NO15/9-A11.

Test nr.	Hydrostatic stress [MPa]	Pore pressure [MPa]	Temperature [°C]
1	5	2	room temp.
2	9	2	room temp.
3	13	2	room temp.
4	7	5	room temp.

The fluid used in all tests was lamp oil.

Compressional wave velocities were measured along the axial direction during the triaxial phase. Input frequency was 500 kHz.

5.2 Data/Results

The effective stress (**σ'**) used in the data analysis is computed from the total/vertical stress (σ_v) minus the pore pressure (**p**) in agreement with Terzaghi's law.

$$\sigma' = \sigma_v - p$$

The reported elastic moduli E (Young modulus) and ν (Poisson ratio) are computed for the tangent at 50% of the triaxial phase on the effective stress curves.

$$E = \left.\frac{d\sigma'}{d\varepsilon_a}\right|_{\sigma'=\frac{1}{2}\sigma'_{peak}}$$

$$\nu = -\left.\frac{d\varepsilon_r}{d\varepsilon_a}\right|_{\sigma'=\frac{1}{2}\sigma'_{peak}}$$

where ε_a and ε_r are the axial and radial deformations.

Velocities were computed from the travel time corrected for system delay (Δt) and the sample length corrected by the axial deformations.

$$V_p = l / \Delta t$$

5.2.1 CU triaxial test

Plots and results from measurement are reported for each test.

Test SACS01

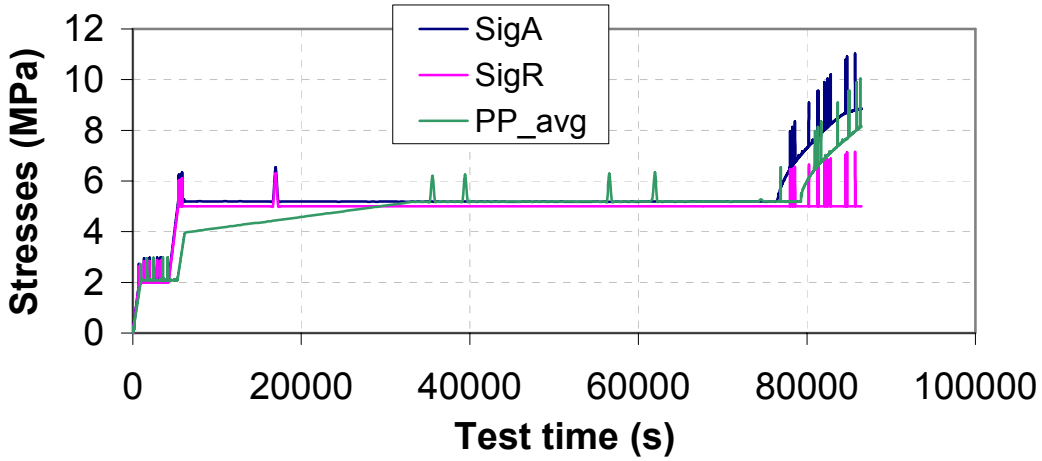

Figure 5.1 *Time evolution of stresses and pore pressure for test SACS02. SigA: stress in axial direction; SigR: stress in radial direction; PP_avg: average pore pressure.*

Figure 5.1 shows that during test SACS01, pore pressure increased up to 5 MPa, i.e. to the level of the confining pressure, instead of being equal to 2 MPa, as planned (see Table 5.1). This implies that the effective stress was equal to 0 (assuming a Biot coefficient of 0). The observed failure of the test occurred due to the weakness of the sample material, which caused the porous plates used for the drainage to become plugged by some of the mobile grains.

Test SACS02

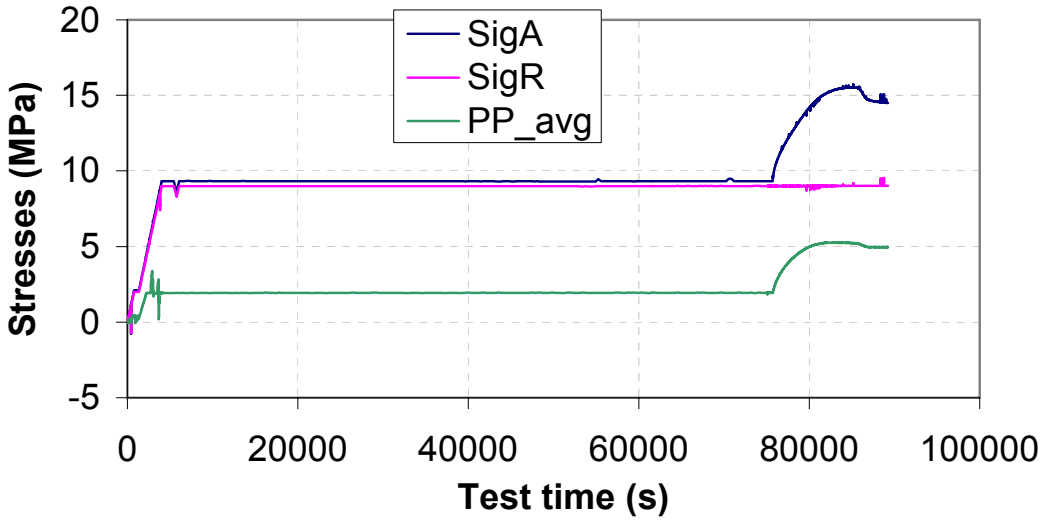

Figure 5.2 *Time evolution of stresses and pore pressure for test SACS02. Abbreviations see Figure 5.1.*

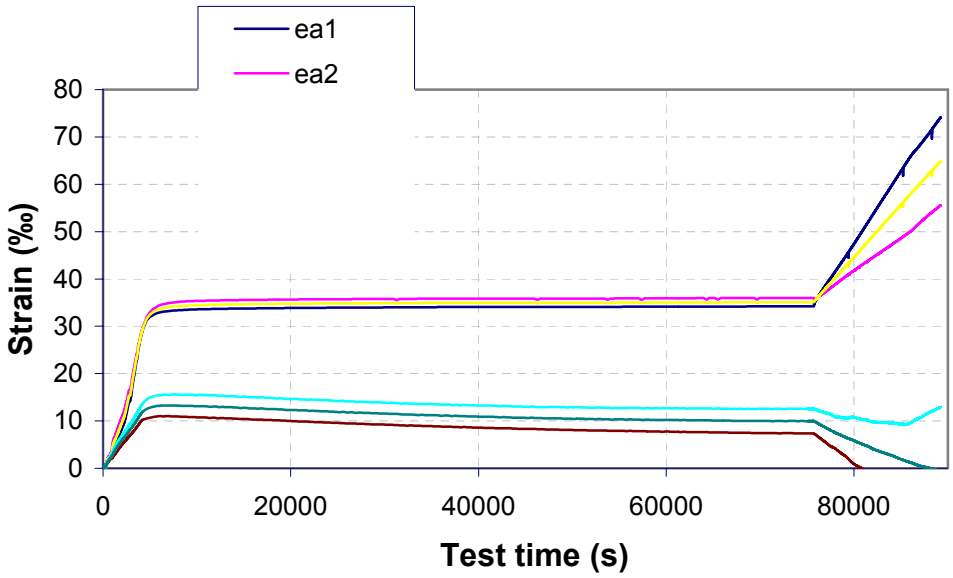

Figure 5.3 *Time evolution of strain measurements for test SACS02. ea1 and ea2: axial strain measurements; ea_avg: average axial strain; et0 and et90: radial strain measurements; et_average: average radial strain.*

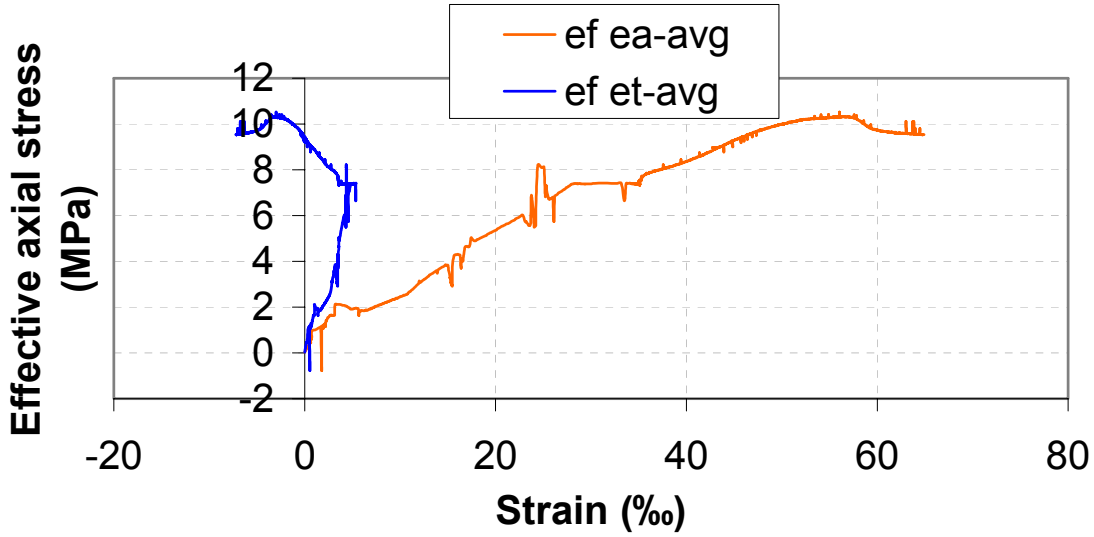

Figure 5.4 *Stress – strain plot for test SACS02. ef ea-avg: effective stress versus average axial strain; ef et-avg: effective stress versus average radial strain*

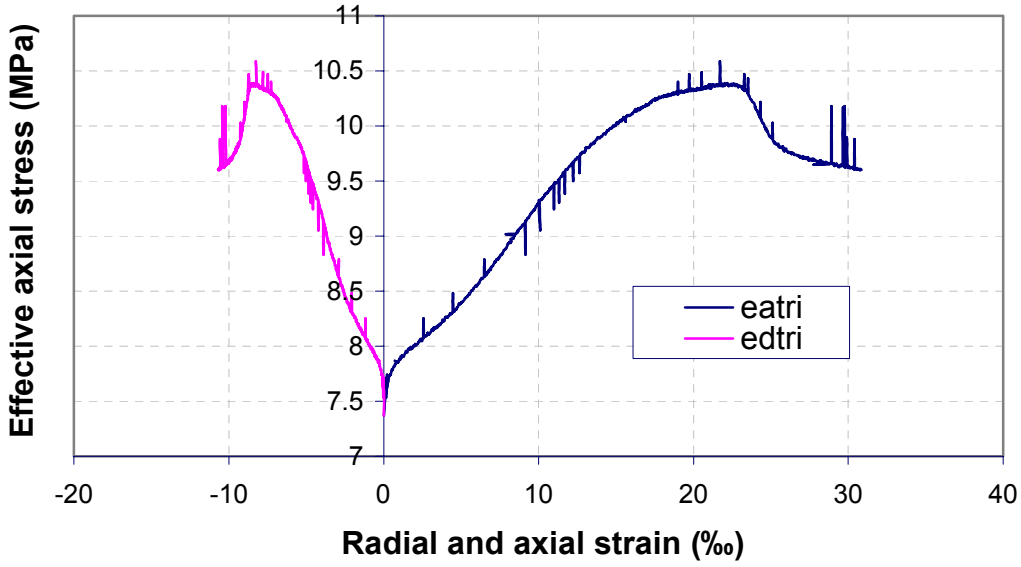

Figure 5.5 *Stress – strain plot for the triaxial phase of test SACS02. eatri: effective axial stress versus axial strain for the triaxial phase; edtri: effective axial stress versus radial strain for the triaxial phase*

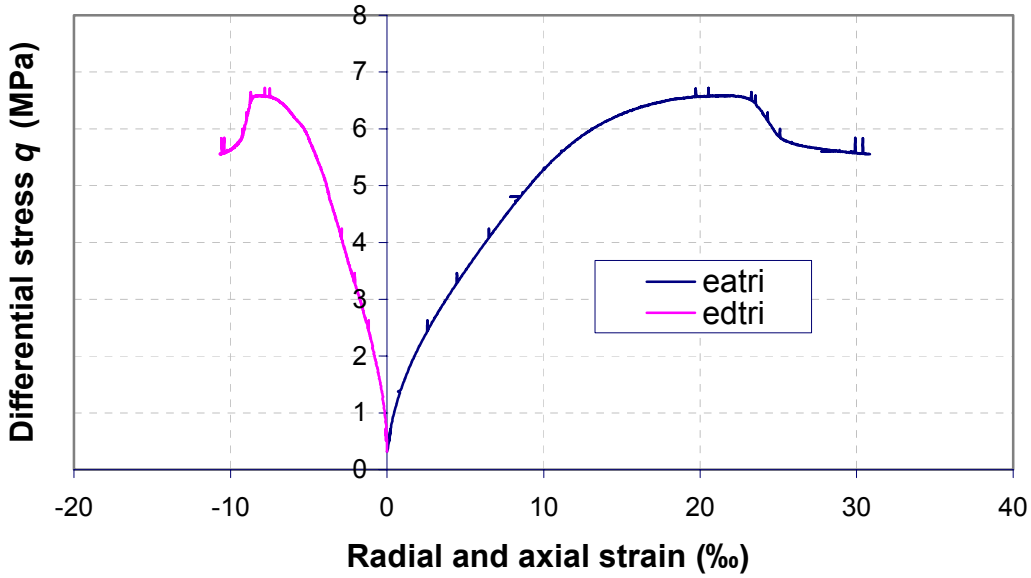

Figure 5.6 *Differential stress q – strain plot for the triaxial phase of test SACS02. eatri: differential stress versus axial strain for the triaxial phase; edtri: differential stress versus radial strain for the triaxial phase*

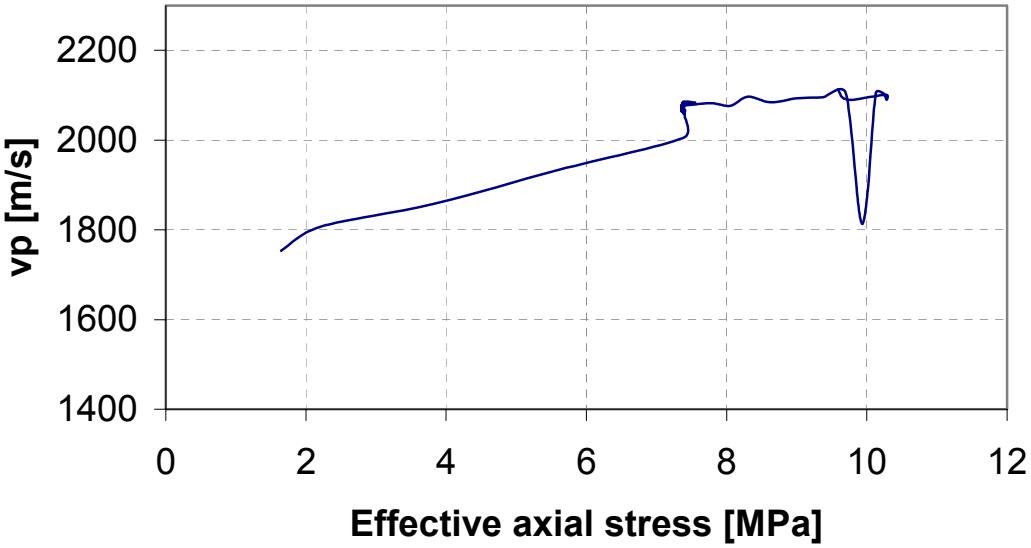

Figure 5.7 *Compressional wave velocity measurement for SACS02*

Velocities increase in the consolidated drained and compaction phases. Generally, this reflects closure of microcracks and compaction, bringing more grains and a larger surface in contact. No significant changes are recorded during the consolidated undrained triaxial phase until failure. This could indicate that dilation compensates stress increase.

Table 5.2 Young's modulus and Poisson's ratio evaluated at half-peak of triaxial phase for test SACS02

Test SACS 02	
E'50	**0.19 ± 0.02 GPa**
ν'50	**0.39 ± 0.01**

The parameters in Table 5.2 are determined by calculating the slopes of the effective axial stress vs. average axial strain and the average radial strain rate vs. average axial strain rate, respectively, for E'50 and ν'50. The uncertainty arises from the choice of the interval length used around $\sigma'_{peak}/2$ to determine these slopes; too short an interval and the inherent coarseness of the stress or strain increase ramp becomes apparent (the press runs up the stress level in discrete steps and the logging points are a discrete distance apart). On the other hand, too long an interval and the slope calculated starts to depart from the ideal tangent slope, as the loading curve is no longer linear at this scale. The error values quoted here are thus specific for this particular loading curve, where the lower and upper limits for the parameters have been tested.

Test SACS03

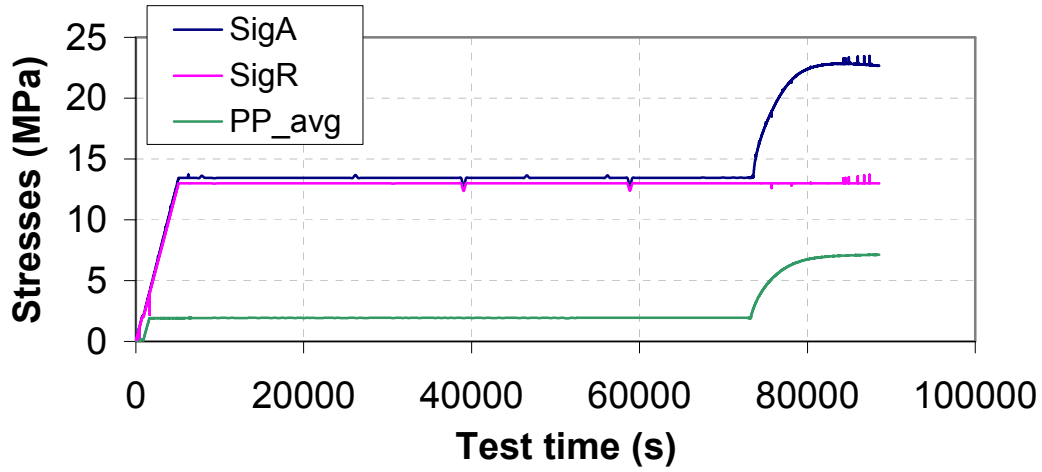

Figure 5.8 Time evolution of stresses and pore pressure for test SACS03. Abbreviations: see Figure 5.1.

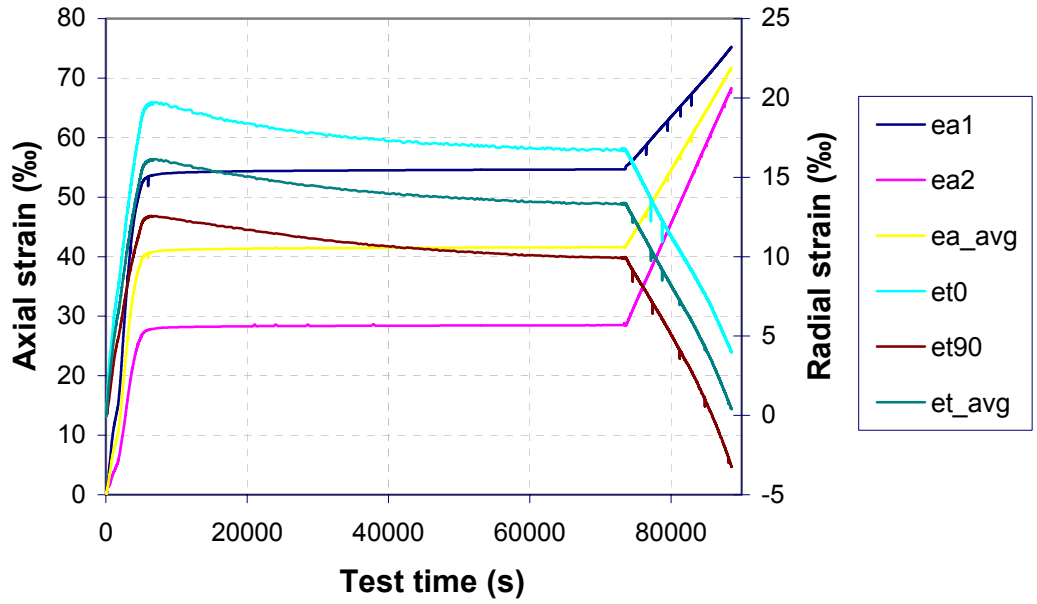

Figure 5.9 *Time evolution of strain measurements for test SACS03. Abbreviations: see Figure 5.3*

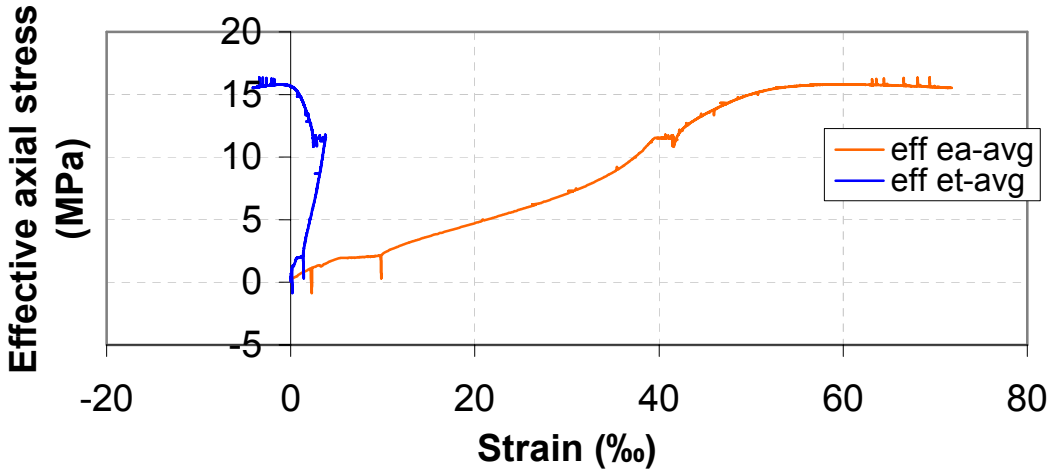

Figure 5.10 *Stress – strain plot for test SACS03. eff ea-avg: effective stress versus average axial strain; eff et-avg: effective stress versus average radial strain*

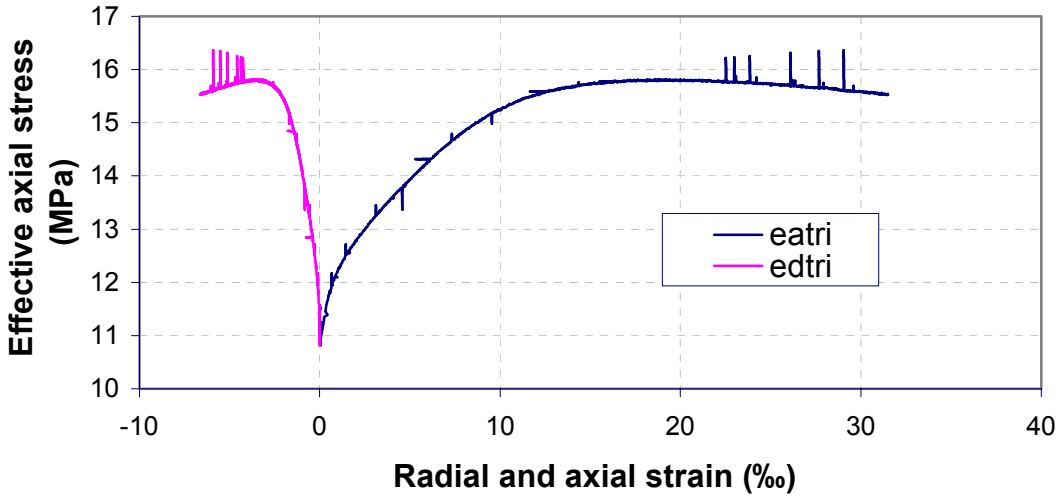

Figure 5.11 *Stress – strain plot for the triaxial phase of test SACS03. Abbreviations: see Figure 5.5.*

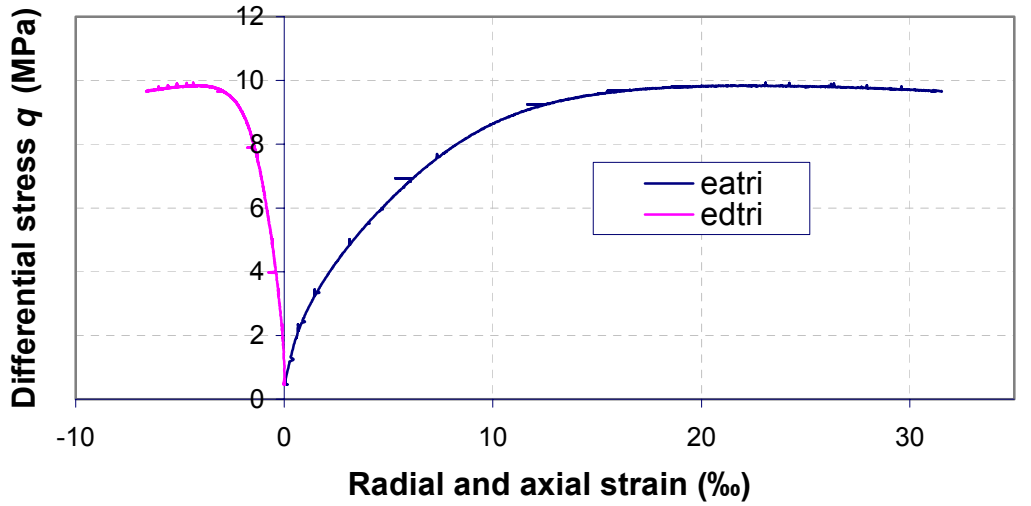

Figure 5.12 *Differential stress q – strain plot for the triaxial phase of test SACS03. Abbreviations: see Figure 5.6*

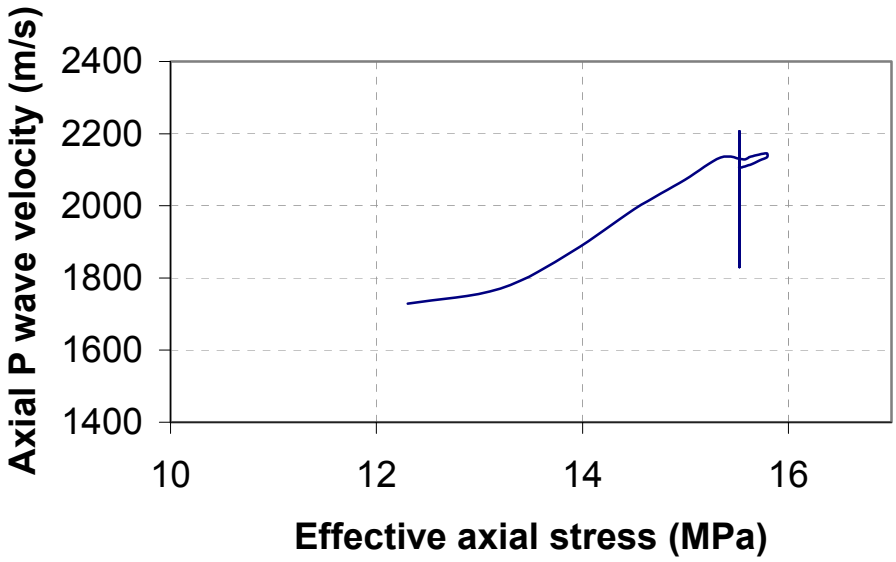

Figure 5.13 Compressional wave velocity measurement for SACS03

Velocities increase during CU triaxial phase. As stated before, this reflects closure of microcracks and compaction, bringing more grains and a larger surface in contact. The saturation seen here corresponds to the flat "peak" in axial stress.

Table 5.3 Young's modulus and Poisson's ratio evaluated at half-peak of the triaxial phase for test SACS03.

SACS03	
E'50	**0.29± 0.02 GPa**
ν'50	**0.18± 0.01**

Again, as in Table 5.2, the parameters in Table 5.3 are determined by calculating the slopes of the effective axial stress vs. average axial strain and the average radial strain rate vs. average axial strain rate, respectively, for E'50 and ν'50. See comment under Table 5.2 concerning the uncertainty calculation.

5.2.2 K_0 Test (Test SACS04)

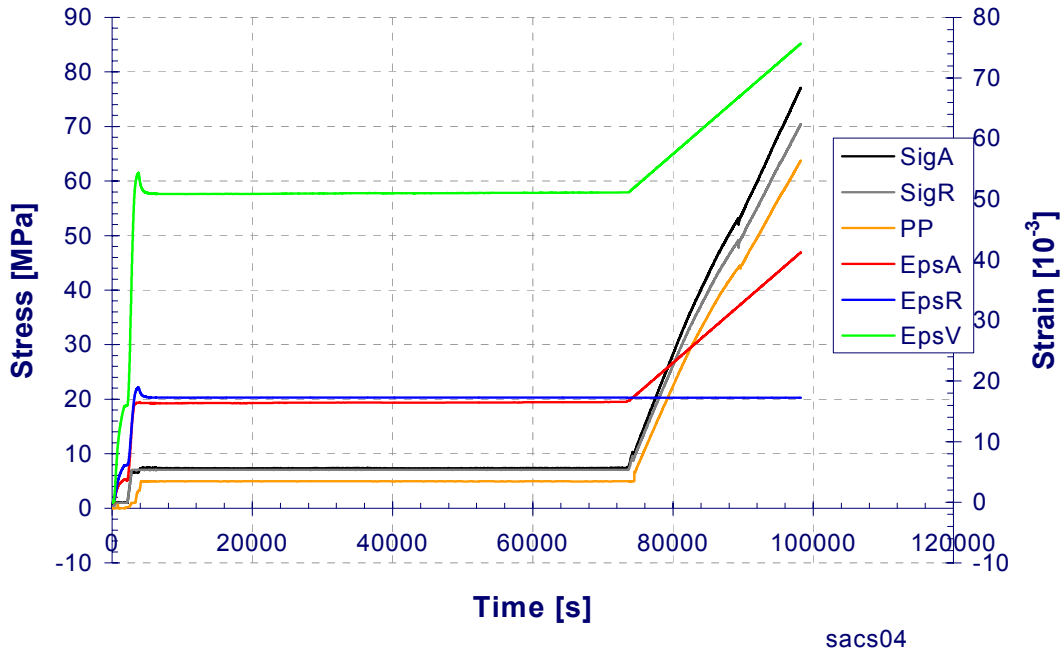

Figure 5.14 Time evolution of stresses, pore pressure and strains for test SACS04. SigA: axial stress; SigR: radial stress; PP: pore pressure; EpsA: axial strain; EpsR: radial strain; EpsV: volumetric strain

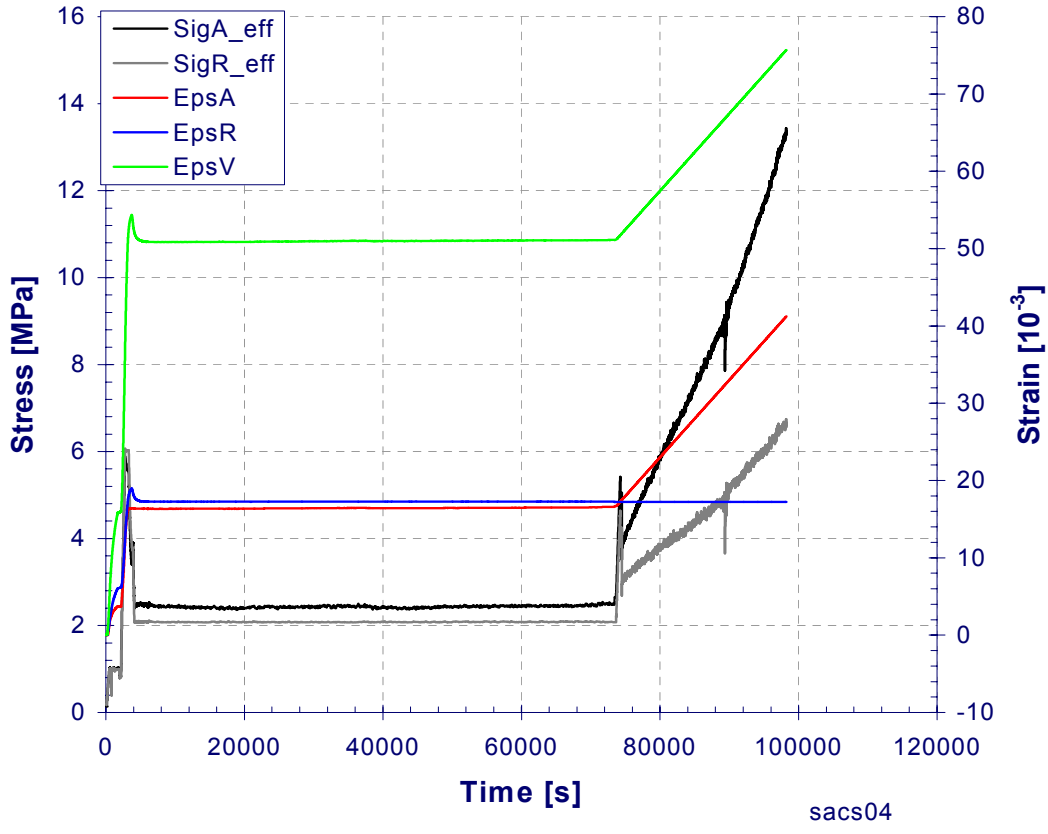

Figure 5.15 Time evolution of effective stresses and strains for test SACS04. Abbreviations: see Figure 5.14. 'eff': effective stress.

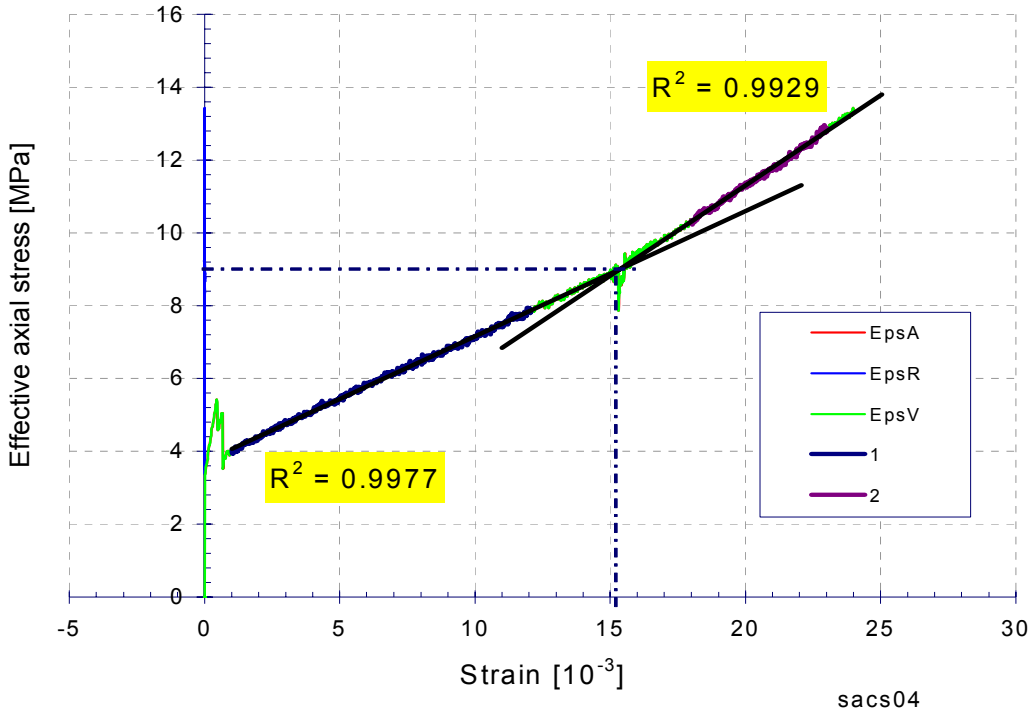

Figure 5.16 *Stress – strain plot for the K_0 phase of test SACS04. The accuracy of the uniaxial strain test can be seen by the strictly 0 radial strain. The inflection of the strain (axial or volumetric) curve suggests an in situ effective vertical stress of ~9 MPa, as shown by the meeting point of the dashed lines. Abbreviations: see Figure 5.14.*

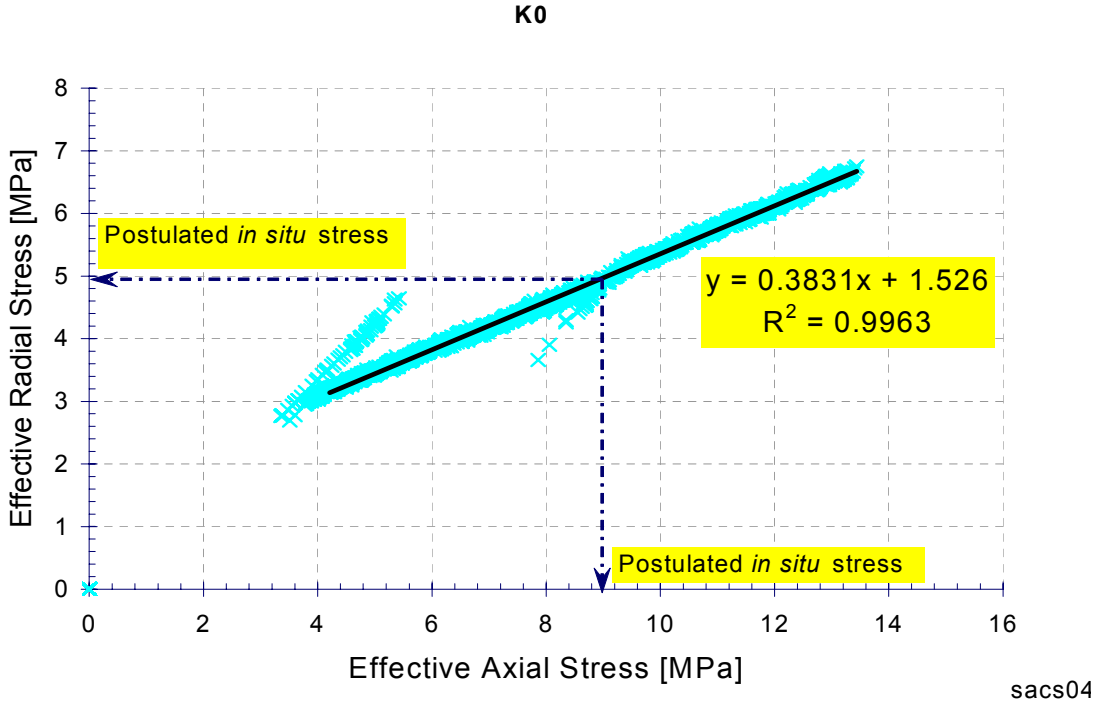

Figure 5.17 *K_0 plot for test SACS04. The in-situ horizontal stress is read to be ~5 MPa, according to the previously determined vertical stress of ~9 MPa (Figure 5.16).*

As seen from Figure 5.16 and Figure 5.17, the estimated *in situ* effective stresses were found from the test to be 9 MPa for the vertical component and 5 MPa for the horizontal component. There are 2 uncertainties associated with the estimation of these stresses: the first one relates to our ability to pick up a well-defined point on the stress – strain curve where the slope changes (see Figure 5.16). The adopted method here relies on tracing linear regressions to the lower and upper stress points separately (the collections of points chosen are labelled "1" and "2", respectively). Extending the resulting straight lines defines the inflection point where they meet. The uncertainty lies in the deviation of the regression coefficient R^2 from its optimal value, 1.

The second source of uncertainty is the general equipment uncertainty, i.e. how precise are the measured values. The load frame is calibrated regularly and corrections are made to account for pressure and load effects: reference tests are run with standard specimens (steel, polymer materials, etc.) with known mechanical properties, whereby any pressure or load dependent deviation from the theoretical results can be captured and accounted for.

Accepting these corrections as valid, intrinsic errors in stress determination remain: for example, if we look at the calculation of effective axial stress, this involves dividing the piston force F_z by the sample's cross section $A = \pi D^2/4$ and subtracting the pore pressure p:

$$\sigma_z^{'} = \frac{4F_z}{\pi D^2} - p$$

so that the combined uncertainty $\delta\sigma_z^{'}$ can be evaluated from the total derivative $d\sigma_z^{'}$:

$$d\sigma_z^{'} = \frac{\partial}{\partial D}\left(\frac{4F_z}{\pi D^2}\right)dD + \frac{\partial}{\partial F_z}\left(\frac{4F_z}{\pi D^2}\right)dF_z - dp$$

$$\delta\sigma_z^{'} = \left|\frac{\partial}{\partial D}\left(\frac{4F_z}{\pi D^2}\right)\right|\delta D + \left|\frac{\partial}{\partial F_z}\left(\frac{4F_z}{\pi D^2}\right)\right|\delta F_z + \delta p$$

The individual uncertainties are as follows: the uncertainty δD on the sample's (initial) diameter is 0.01 mm, which is the resolution of the digital calliper used; the relative uncertainty $\delta F_z/F_z$ for the axial force is given by the manufacturer to be 0.05 %, while the last uncertainty term for the pressure transducer reading the pore pressure is probably the worst at typically 0.5 %.

The total relative uncertainty calculated for an effective stress of 10 MPa is thus the sum of the 3 components: 0.02 % for the term involving the derivative with respect to the diameter D, 0.02 % again for the term involving the derivative with respect to the piston force and 0.5 % for the last term (pressure transducer), or in total less than 1 %. The calculation was based on the value of 5 kN for the force read for the 10 MPa output, and a diameter of 0.038353 m at this stress, yielding an absolute error of 2 kPa each for the first 2 uncertainty components.

6. Discussion and conclusion

The very weak and ductile nature of this caprock shale is clearly apparent from the mechanical testing: the first test at low confining stress, test SACS01, failed because the sample "flowed" through the serrated plate, thus plugging it; all the successful strain-stress curves shown above (the triaxial portion of the tests) emphasise an almost elastic-perfectly plastic behaviour, with almost no reduction in strength in the post – peak region.

The Young's modulus at half peak stress (E_{50}) was found to increase from 0.2 GPa to 0.3 GPa with increasing confinement (tests SACS02 and SACS03). These values are more than an order of magnitude lower than typical values for deep shales (over 3 km depth) where for the same confinement values one gets 4 – 6 GPa. Similarly, the Poisson's ratio at half-peak (ν_{50}) decreases from 0.4 to 0.2 with increasing confinement, which is as expected. Comparing with deeper shales, we find the values to be quite similar.

From the K_0 test (Figure 5.16), it appears that the in situ vertical effective stress we infer from the slope change in the stress – strain domain correlates poorly to the expected value: from the tests we find a probable value of 9 MPa while the calculations indicated a value in the range 6 to 7 MPa (see Appendix B). One possible explanation for this discrepancy may be previous additional load exerted by an ice sheet. An ice sheet resting on the sea floor, and rising 200 m above seal level, would cause an additional effective stress of approximately 2 MPa.

In any case, the K_0 plot allows us to give a corresponding value for the expected in situ horizontal effective stress, situating it either at 4 or 5 MPa (Figure 5.17), depending on the value chosen for the vertical effective stress.

It must be stressed that in order to yield results relevant to in situ conditions, the cores were taken such that their axis would be parallel to the in situ vertical direction. However, some uncertainty in the true angle of the core relative to vertical at this depth remains, as well as some uncertainty relative to the bedding plane inclination. Small angle variations may give relatively large strength differences.

7. References

Arts, R., Chadwick, A., Eiken, O., & Zweigel, P., 2003: Interpretation of the 1999 and 2001 time-lapse seismic data (WP5.4). TNO-report NITG 03-064-B, 32pp. (www-link)

Bøe, R. & Zweigel, P. 2001: Characterisation of the Nordland Shale in the Sleipner area by XRD analysis – A contribution to the Saline Aquifer CO2 Storage (SACS) project. SINTEF Petroleum Research report 33.0764.00/01/01. Confidential. 23pp. (www-link)

Cerasi, P., Bøe, R., Sønstebø, E.F., & Larsen, I., 2003: Statoil Smørbukk shale laboratory programme: triaxial and hollow cylinder tests. SINTEF Petroleum Research report 33.5336.00/01/03. Confidential. 113pp. (www-link)

Fjær, E, Holt, R.M., Horsrud, P., Raaen, A.M. & Risnes, R. 1996: Petroleum related rock mechanics. Developments in Petroleum Science, 33, 2nd print. Elsevier, 338pp.

Kemp, S.J., Bouch, J. & Murphy, H.A. 2001: Mineralogical characterisation of the Nordland Shale, UK Quadrant 16, northern North Sea. British Geological Survey Commissioned Report, CR/01/136. Confidential, 52pp. (www-link)

Kemp, S.J., Pearce, J.M. & Steadman, E.J. 2002: Mineralogical, geochemical and petrographical characterisation of Nordland Shale cores from well 15/9-A11, Sleipner field, northern North Sea. British Geological Survey Commissioned Report, CR/02/313. Confidential, 40pp. (www-link)

Lindgren, H., Fries, K. & Springer, N. 2002: Saline Aquifer CO2 Storage Project, SACS, Phase II – Task 1.4: Evaluation of cap rock sealing the reservoir – Clay mineralogical investigations of core and cuttings from the Ekofisk and Sleipner areas. Danmarks og Grønlands Geologiske Undersøgelse Rapport 2002/3. Confidential, 10pp. (www-link)

Zweigel, P. & Hamborg, M. 2002: The effect of time-depth conversion procedure on key seismic horizons relevant for underground CO_2 storage. - A contribution to the Saline Aquifer CO2 Storage (SACS) project. SINTEF Petroleum Research report 33.5324.00/01/02. Confidential, 48pp. (www-link)

8. Appendix A: Core photographs

Figure 8.1 Core segment 1 (907.80 to 908.80 m MD) - overview

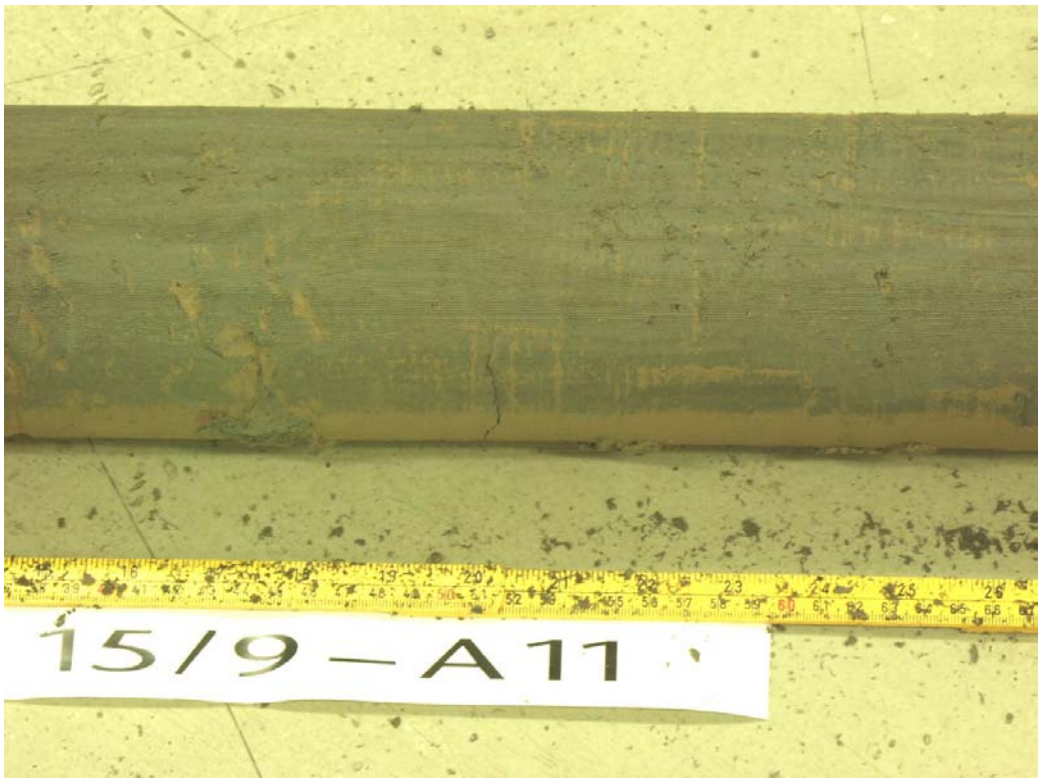

Figure 8.2 Central part of core segment 1 (907.80 to 908.80 m MD).

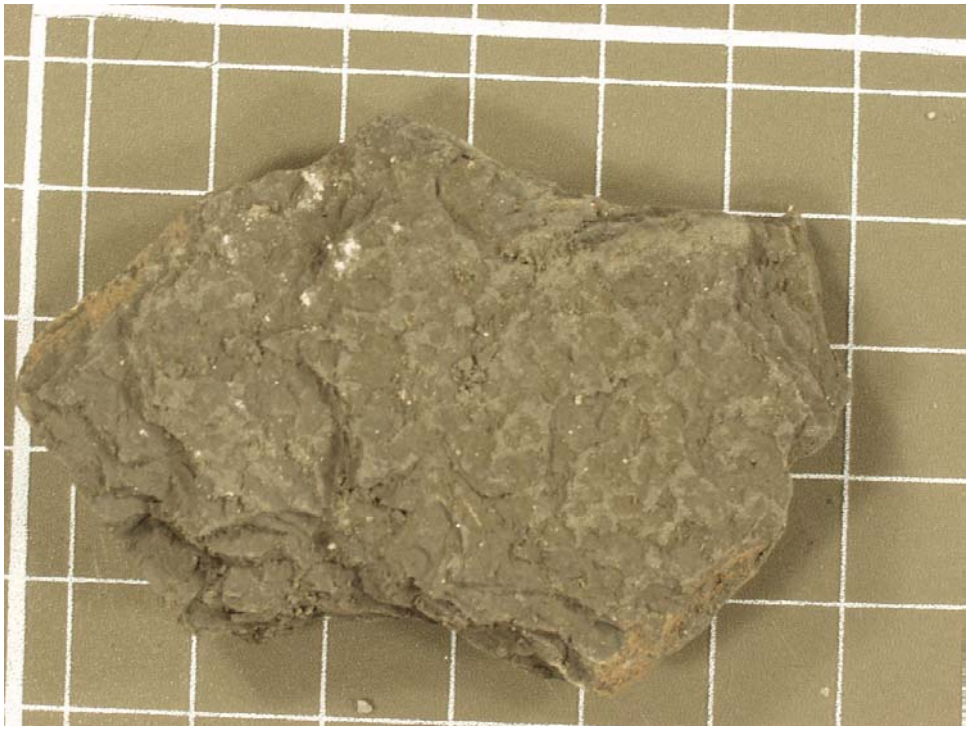

Figure 8.3 *Sample from upper end of core segment 1. Scale in cm. View on surface at which sample split from core, parallel to core axis. Bedding would be expected to be cut by this surface.*

Figure 8.4 *Sample from upper end of core segment 1. Scale in cm. View parallel to surface at which sample split from core. Bedding would be expected to be cut by this surface. Visible fabric is subparallel to split surface, i.e. roughly parallel to core axis.*

Figure 8.5 Lower part of core segment 1. Probably damaged by coring process.

Figure 8.6 Core segment 2 (911.60 to 912.60 m MD) - overview

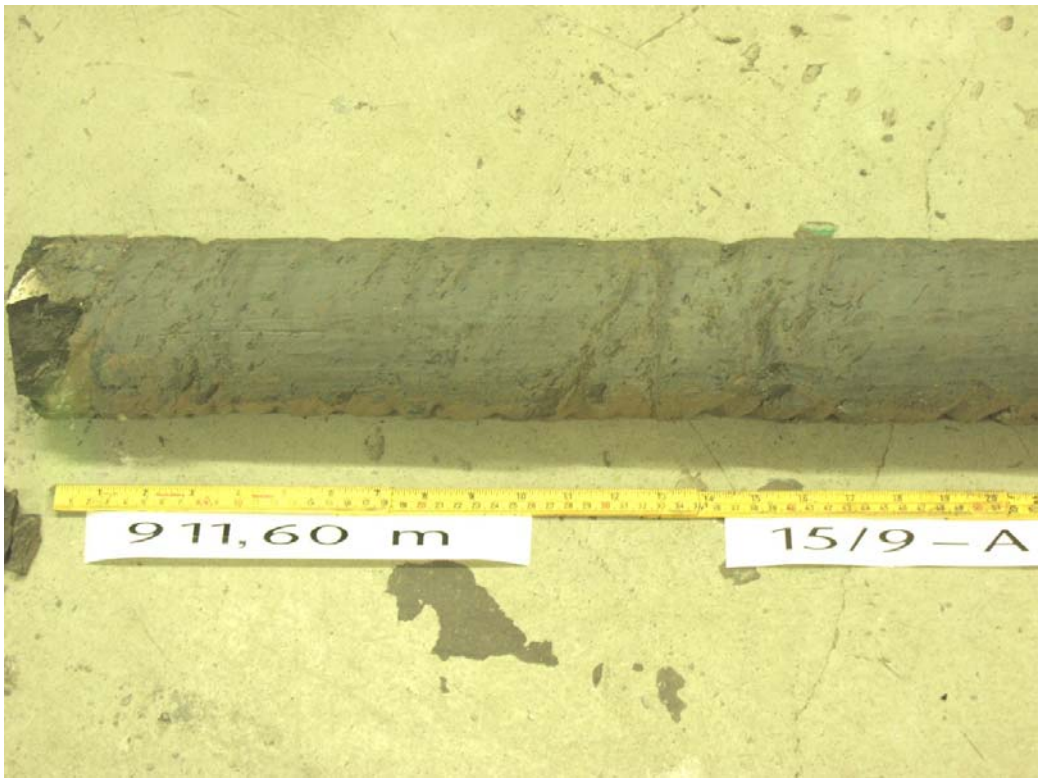

Figure 8.7 *Upper end part of core segment 2. Note stripes by blackish spots arranged in lines from lower left to upper right – these may be bedding.*

Figure 8.8 *Lower end part of core segment 2. Note fracture at left side and hole in core on upper side of photograph.*

Figure 8.9 Core segment 3 (912.60 to 913.10 m MD) – overview.

Figure 8.10 View on fault plane in core segment 3 at approx. 912.8 m MD. Fault plane dips towards upper side of photograph. Note slip lines on fault plane.

9. Appendix B: In-situ stress and pressure in the Sleipner case

The shale samples from well 15/9-A11 in the Sleipner area are from approximately 785 m TVDss. Water depth in the area is approximately 80 m.

Burial depth, i.e. thickness of the overburden, is accordingly approximately 705 m.

Effective pressure (effective vertical stress) can be calculated from lithostatic pressure (σ_{Lith}) and pore pressure (p) by

(1) $$\sigma' = \sigma_{Lith} - p$$

Lithostatic pressure is

(2) $$\sigma_{Lith} = \rho_{rock} \cdot h \cdot g + p_{seafloor}$$

with ρ_{rock} being average rock density of the overburden, h being the thickness of the overburden, g being the gravitational acceleration, and $p_{seafloor}$ being the water pressure at the sea floor, which can be calculated using

(3) $$p = \sigma_{hydr} = \rho_{water} \cdot z \cdot g$$

with ρ_{water} being the average formation and sea water density, z the depth below sea level, and g being the gravitational acceleration.

There are no indications for overpressure in the Utsira Sand in the Sleipner area, and pore pressure can therefore be calculated as the hydrostatic pressure with equation (3).

For water densities of 1.00 to 1.05 g/cm^3 and average overburden rock densities of 1.9 - 2.0 g/cm^3 this yields effective vertical stresses ranging approximately between 6 and 7 MPa (Table 9.1).

Table 9.1: Vertical effective stress calculated for the sample depth of shale samples from well 15/9-A1, based on a simple overburden density model.

Water density [g/cm^3]	Bulk rock density [g/cm^3]	Vertical effective stress at 785 mTVDss [MPa]
1	1.9	6.22
1	2	6.92
1.05	1.9	5.88
1.05	2	6.57